Estimates of Anthropogenic Carbon in the Indian Ocean with Allowance for Mixing and Time-Varying Air-Sea CO_2 Disequilibrium

Timothy M. Hall
NASA Goddard Institute for Space Studies and Columbia University, New York, NY

Darryn W. Waugh
Johns Hopkins University, Baltimore, MD

Thomas W. N. Haine
Johns Hopkins University, Baltimore, MD

Paul E. Robbins
Scripps Institution of Oceanography, UCSD, San Diego, CA

Samar Khatiwala
Lamont-Doherty Earth Observatory, Columbia University, Palisades, NY

Abstract. We apply to the Indian Ocean a novel technique to estimate the distribution, total mass, and net air-sea flux of anthropogenic carbon. Chlorofluorocarbon data are used to constrain distributions of transit times from the surface to the interior that are constructed to accommodate a range of mixing scenarios, from no mixing (pure bulk advection) to strong mixing. The transit-time distributions are then used to propagate to the interior the surface-water history of anthropogenic carbon estimated in a way that includes temporal variation in CO_2 air-sea disequilibrium. By allowing for mixing in transport and for variable air-sea disequilibrium, we remove two sources of positive bias common in other studies. We estimate that the anthropogenic carbon mass in the Indian Ocean was 14.3–20.5 Gt in 2000, and the net air-sea flux was 0.26–0.36 Gt/yr. The upper bound of this range, the no-mixing limit, generally coincides with previous studies, while the lower bound, the strong-mixing limit, is significantly below previous studies.

1. Introduction

The ocean sequesters a large fraction of the CO_2 arising from human activity. While great progress has been made estimating the distribution and mass of anthropogenic carbon in the ocean from observations, considerable uncertainty remains. The task is difficult because the anthropogenic signal of dissolved inorganic carbon (ΔDIC) is order 100 times smaller than natural DIC, which has complex, poorly-known biochemical sources and sinks. Various ΔDIC inference techniques have been developed [*Brewer*, 1978; *Chen and Millero*, 1979; *Gruber et al.*, 1996; *Goyet et al.*, 1999; *Thomas and Ittekkot*, 2001; *McNeil et al.*, 2003], and, while comparison among them show qualitative agreement, there are considerable quantitative differences [*Wanninkhof et al.*, 1999; *Sabine and Feely*, 2001; *Coatanoan et al.*, 2001].

Paper number .
0886-6236/04/$12.00

Several assumptions are common to most ΔDIC inference techniques, raising the possibility of overall bias across the range of estimates. Chief among these are 1, the assumption that mixing is a negligible component of transport; and 2, the assumption of "constant disequilibrium" that ΔDIC in surfaces waters has kept pace with increasing atmospheric CO_2. Both of these assumptions have been questioned, but the errors incurred by making them have remained unclear. A number of studies have demonstrated that eddy mixing along constant density surfaces (isopycnals) plays a major role in propagating tracers [e.g., *Jenkins*, 1988; *Robbins et al.*, 2000] and must be taken into account when interpreting tracer-derived timescales [e.g., *Thiele and Sarmiento*, 1990; *Sonnerup*, 2001; *Waugh et al*, 2003a]. Information on the mixing, however, has not generally been incorporated in the observationally-based ΔDIC estimates. In addition to the weak-mixing and constant-disequilibrium assumptions, techniques that derive ΔDIC from total DIC measurements account for biochemical sources and sinks of DIC by using stoichiometric (Redfield) ratios among carbon, oxygen and alkalinity, whose uncertainty impacts the ΔDIC estimates [*Wanninkhof et al.*, 1999].

In this study we apply to the Indian Ocean a technique that avoids these assumptions. As in other studies, we exploit the fact that ΔDIC is well approximated as a passive,

inert tracer transported by a steady-state circulation on surfaces of constant density (isopycnals) in response to anthropogenic forcing in surface waters. Unlike other studies we relate interior ΔDIC to the ΔDIC history at the surface in a way that explicitly allows for mixing. CFC12 data are used to constrain distributions of transit times from the surface to the interior that are designed to accommodate any proportion of diffusive mixing and bulk advection. The transit-time distributions are then used to propagate to the interior the surface history of ΔDIC estimated in a manner that allows for time-varying CO_2 disequilibrium. The assumptions of no-mixing and constant-disequilibrium both lead to positive bias. By removing them we obtain a range of values for Indian Ocean mass and net air-sea flux of anthropogenic carbon, all of which are consistent with the CFC data. The upper limit of the range approximately coincides with previous studies, while the lower limit is roughly one-third lower.

2. Methodology

We exploit the approximation, also made in other studies, that ΔDIC penetrates the ocean as a passive, inert tracer. This is reasonable, because, while the distribution of DIC itself is controlled by biology, upper ocean productivity is limited by nutrients not carbon, and thus to first order the addition of anthropogenic carbon does not alter the rate of biological uptake and downward transport of carbon. Furthermore, as in other studies, we assume the ocean circulation to be in steady-state. *McNeil et al.* [2003] estimated from model studies that present day secular change in the ocean circulation due to global warming alters carbon uptake by only $\sim 1\%$. Decadal and shorter-time variability in the interior ocean does not affect our analysis significantly because many decades of tracer signal are integrated [*Hall et al.*, 2002]. However, annual and interannual variability of the outcrops of isopycnals causes uncertainty in estimating the histories surface waters of ΔDIC and CFC12 (see Section 3.2).

We make use of the following relationship valid for any passive, inert tracer transported by a steady-state circulation in response to a uniform time-dependent surface forcing:

$$c_V(t) = \int_0^\infty c_S(t-t')\mathcal{G}_V(t')dt' \qquad (1)$$

where $c_S(t)$ is the tracer concentration assumed to be uniform on the surface region S, and c_V is the concentration averaged over a volume V that includes S. $\mathcal{G}_V(t)$ is the distribution of transit-times since the water in V last made contact with S, where it was labeled by tracer [*Beining and Roether*, 1996; *Haine and Hall*, 2002]. The mean tracer concentration in the volume is comprised of all the past contributions on the surface, weighted by $\mathcal{G}_V$. The shape of $\mathcal{G}_V(t)$, determined by the nature of the transport, will be estimated by CFC12 observations and inversion of (1) in the following section.

While relationship (1) can be generalized to include spatially-varying tracer concentration on the surface [*Haine and Hall*, 2002], uniform concentration on the surface is a good approximation in this application. The main thermocline of the Indian Ocean is ventilated predominantly from the south, either through winter subduction or mode water formation [*Karstensen and Quadfasel*, 2002], and anthropogenic tracers (or any air-sea flux anomaly) penetrate the upper ocean along isopycnals [*Fine et al.*, 1981]. Thus, we can apply relationship (1) separately to northward transport along each isopycnal in response to time-varying tracer concentrations at the southern outcrop. Finally, because temperature is the most important factor determining both the solubilities of the tracers we consider and the density of sea-water, tracer concentrations are approximately uniform along the outcrops.

We neglect sources of water from the Red Sea. The volume flux from these sources is only 1%–2% of the southern source [*Karstensen and Quadfasel*, 2002; *Bower et al.*, 2000], but because of the high temperature and salinity their fractional ΔDIC contribution may be higher. (The solubility of DIC decreases with T and S, but ΔDIC increases, due to nonlinearities in DIC's dependence on T, S, alkalinity and atmospheric CO_2.) The error incurred by this neglect is estimated in section 3.2.

Our analysis is performed separately on 15 isopycnals, the deepest of which ($\sigma_0 = 27.65$) reaches an approximate depth of 1500 m in southern midlatitudes. We find that the contribution to the total inventory decreases rapidly with density, with $\sigma_0 = 27.65$ containing less than 2% of the total ΔDIC (compared to $\sigma_0 = 26.7$, which contains 17% of the total). We assume that deeper isopycnals contribute insignificantly. North of 35°S the Indian Ocean is defined by its bounding land masses, while to the south it includes the sector of the Southern Ocean between 20°E and 120°E. The volumes V in expression 1, over which the tracer concentrations are averaged, are defined vertically by the separation of adjacent isopycnals, to the south by the outcrop regions (surfaces S) of the isopycnals, and to the north by surfaces of constant concentration, c, of a specified tracer. A series of successively larger volumes is thereby defined as a function of c, the largest being the volume of the entire isopycnal slab. This formulation allows us to construct spatial distributions of ΔDIC, while at the same time enforcing certain global constraints (see below).

2.1. Constraining $\mathcal{G}_V(t)$

To apply relationship 1 to ΔDIC we need $\mathcal{G}_V(t)$ and $\mathrm{DIC}_S(t)$, the history of ΔDIC at the surface. $\mathcal{G}_V(t)$ is obtained by inverting relationship 1 using observations of another passive, inert tracer, CFC12, that has no natural background and a well-known atmospheric history. CFC12 data from the World Ocean Circulation Experiment (WOCE) Indian Ocean cruise lines of 1994–1996 have been objectively mapped onto the isopycnal surfaces, and these $1° \times 1°$ gridded data are used in our analysis. The surface outcrops are taken to be the intersection of the isopycnal with the surface. An example is shown in Fig. 1. CFC12 concentrations are largest at the southern outcrop and decrease to the north. The deepest isopycnals considered have negligible CFC12 through much of the northern Indian Ocean. To obtain the surface history at the outcrops, $\mathrm{CFC12}_S(t)$, we use the atmospheric history [*Walker et al.*, 2000] scaled to match the observed 1995 outcrop CFC12 concentrations. In this way the degree of saturation at the outcrop is approximately included in $\mathrm{CFC12}_S(t)$. However, there is considerable uncertainty in $\mathrm{CFC12}_S(t)$, as the outcrop location and CFC12 saturation vary seasonally, and the observations are generally not taken at the time of subduction.

We apply (1) to CFC12 and invert for $\mathcal{G}_V(t)$ parametrically. The following functional form of two parameters is assumed:

$$\mathcal{G}_V(t) = \frac{1}{\sqrt{\pi P \tau^2 t}} \left(e^{-Pt/4\tau} - e^{-P(\tau-t)^2/4\tau t} \right) + \frac{1}{2\tau} \left(\mathrm{erf}\left(\sqrt{\frac{Pt}{4\tau}} \right) + \mathrm{erf}\left(\sqrt{\frac{P}{4\tau t}} (\tau - t) \right) \right) \quad (2)$$

where τ is a timescale equal to twice the mean transit time ("mean age") of all the fluid elements in V and $P = UL/\kappa$ is the Peclet number, given a characteristic velocity scale U, length scale L and diffusivity κ. Large P corresponds to weak mixing. We discuss and illustrate this functional form in the appendix.

A range of transport scenarios, from no mixing and rapid bulk advection to strong mixing and slow bulk advection, are consistent with the CFC12 observations, and thus CFC12 can at most constrain $\mathcal{G}_V(t)$ to a family of functions. Fig. 2a shows examples of $\mathcal{G}_V(t)$ at different parameter values, all of which produce the same volume-averaged concentration, $\mathrm{CFC12}_V$, when combined with $\mathrm{CFC12}_S(t)$ via relationship (1). In the high P limit (no mixing) water and tracer march unmixed from the outcrop to the volume edge. All transit times less than τ, the time to reach the volume edge, are represented with equal mass proportion, and no tracer is found at transit times greater than τ. In the low P limit (strong mixing) $\mathcal{G}_V(t)$ heavily weights short transit times, due to rapid recirculation with the surface, but also has a long tail that extends well past τ, due to meandering pathways from the surface. An observation of $\mathrm{CFC12}_V$, coupled with $\mathrm{CFC12}_S(t)$, constrains τ and P to a locus of points (Fig. 2b).

2.2. Applying $\mathcal{G}_V(t)$ to ΔDIC

To obtain $\Delta\mathrm{DIC}_S(t)$ we begin with (but subsequently relax) the widely-made "constant disequilibrium" assumption that anthropogenic CO_2 in the atmosphere ($\Delta\mathrm{CO}_2(t)$) and $\Delta\mathrm{DIC}_S(t)$ evolve in lock-step, so that one may be obtained from the other using equilibrium carbon chemistry. In making the constant disequilibrium assumption, it is recognized that locally CO_2 across the air-sea interface is not in chemical equilibrium, but it is assumed that the degree of disequilibrium has not changed significantly since preindustrial times. Following *Thomas et al.* [2001], we form the difference time series $\Delta\mathrm{DIC}(t) = \mathrm{DIC}(t) - \mathrm{DIC}(1780)$, where the year 1780 is selected as the start of the industrial era. (This definition is chosen for consistency with other studies. In 1780 ice-core records indicate that atmospheric CO_2 concentrations were about 280 ppm [*Etheridge et al.*, 1998], which is the preindustrial level assumed by *Sabine et al.* [1999] and others. Estimates of instantaneous air-sea fluxes are not affected by the choice of preindustrial level.) The "disequilibrium term", assumed to be constant, is present in both terms of the difference, and so cancels, leaving only the equilibrium terms. We can therefore solve the well-documented equilibrium inorganic chemistry system [e.g., *Lewis and Wallace*, 1988] to compute $\Delta\mathrm{DIC}_S(t)$, given observations of temperature, salinity, alkalinity, and atmospheric $\Delta\mathrm{CO}_2(t)$. In these calculations we use the carbonate dissociation coefficients of *Goyet and Poisson* [1989]. Use of other published coefficients makes a negligible difference in our estimates.

The $\Delta\mathrm{DIC}_S(t)$ is convolved with $\mathcal{G}_V(t)$ for a range of τ and P, resulting in contours of volume-averaged concentration, $\Delta\mathrm{DIC}_V$ (Fig. 2b). The intersection of $\Delta\mathrm{DIC}_V$ contours by a particular $\mathrm{CFC12}_V$ contour is the constraint that the $\mathrm{CFC12}_V$ observation imposes on $\Delta\mathrm{DIC}_V$. Note that the ranges of τ and P are chosen large enough that the $\mathrm{CFC12}_V$ and $\Delta\mathrm{DIC}_V$ contours are parallel in the low and high limits. Any additional range of parameters results in no additional change in $\Delta\mathrm{DIC}_V$ for a given $\mathrm{CFC12}_V$. The minimum (strong-mixing) to maximum (no-mixing) range of $\Delta\mathrm{DIC}_V$ as a function of $\mathrm{CFC12}_V$ obtained from the contour intersections is shown in Fig. 2c. The tracer concentrations are expressed as fractions of their contemporary outcrop values, which renders the CFC12-ΔDIC relationship independent of the isopycnal.

Because we assume steady-state circulation, $\mathcal{G}_V(t')$ in equation (1) depends on transit time t', but not on calendar date, t. Therefore, once $\mathcal{G}_V(t')$ is constrained it can be applied to ΔDIC, via (1), at any t. In this way, at each calendar year t we compute for each isopycnal, σ, the mass $\Delta M^{\sigma}_{DIC} = V_\sigma \times \Delta\mathrm{DIC}_{V_\sigma}$, where V_σ is the volume of the entire isopycnal slab. Summing over all isopycnals, we then have the history over the industrial era of anthropogenic carbon mass, $\Delta M_{DIC}(t)$, in the Indian Ocean, as well as the net air-sea flux, $\Delta F_{DIC}(t) = d\Delta M_{DIC}/dt$, into the Indian Ocean, at constant equilibrium (Fig. 3).

2.3. Time-Varying CO_2 Disequilibrium

The assumption of constant disequilibrium is erroneous. If the ocean was on average in equilibrium with the atmosphere in the preindustrial era, but is now taking up some fraction of anthropogenic carbon, then the mean disequilibrium must have changed. It is the disequilibrium, the difference in CO_2 across the air-sea interface, that drives the net air-sea flux. The anthropogenic component of the flux into isopycnal σ is

$$\Delta F^{\sigma}_{DIC}(t) = k(\Delta CO_2(t) - \alpha \Delta\mathrm{DIC}_S(t)) \quad (3)$$

where α is the equilibrium chemistry factor (dependent on temperature, salinity, and alkalinity) that converts DIC_S to the atmospheric CO_2 with which it would be in equilibrium; and k is the transfer coefficient, dependent on solubility and wind speed. If the disequilibrium has remained constant since the preindustrial era, then $\Delta CO_2(t) - \alpha\Delta\mathrm{DIC}_S(t) = 0$ and $\Delta F^{\sigma}_{DIC}(t) = 0$, inconsistent with the nonzero flux computed by assuming constant disequilibrium in the CFC12 method (Fig. 3).

In order to resolve this inconsistency, we must modify $\Delta\mathrm{DIC}_S(t)$ and $\Delta F^{\sigma}_{DIC}(t)$ until they satisfy both equation 3 and our relationship between $\Delta\mathrm{DIC}_S(t)$ and $\Delta F^{\sigma}_{DIC}(t)$ via the CFC12-constrained $\mathcal{G}_V(t)$. That is, on each isopycnal σ we have two unknowns, $\Delta\mathrm{DIC}_S(t)$ and $\Delta F^{\sigma}_{DIC}(t)$, for which we solve simultaneously using the following two equations: expression (3) and

$$\Delta F^{\sigma}_{DIC}(t) = \frac{d}{dt} \left(V_\sigma \int_0^\infty \Delta\mathrm{DIC}_S(t - t') \mathcal{G}_V(t') dt' \right), \quad (4)$$

the expression for the flux as the time rate of change of the mass obtained from $\Delta\mathrm{DIC}_S(t)$ via the CFC12-constrained

$\mathcal{G}_V(t)$. Equating (3) and (4) is the statement that the flux into the isopycnal slab must equal the mass rate of change within the slab and provides an integral equation for $\Delta\mathrm{DIC}_S(t)$, which can be solved iteratively using the constant-disequilibrium history as the first guess. Once $\Delta\mathrm{DIC}_S(t)$ is obtained, $\Delta F_{DIC}(t)$ can be computed from (4).

In this solution we use values for the transfer coefficient k estimated by *Carr et al.* [2002], who employed the *Wanninkhof* [1992] wind speed parameterization and wind speeds from both SSM/I and QuickSCAT scaterometer data. In addition, we require the areas A of the outcrop regions, which we take to equal the areas between surface CFC12 contours at the sourthern extremities of adjacent isopycnals. Importantly, our mass and net air-sea flux estimates are relatively insensitive to the large uncertainty in k and A, because the correction due to the relaxation of constant disequilibrium, shown in section 3, is small. For example, $\pm 50\%$ uncertainty in k causes approximately $\pm 5\%$ uncertainty in ΔDIC mass and flux. The uncertainty in k impacts the magnitude of a first order correction, but not the zero order estimate.

2.4. Computing Spatial Distributions

In the calculation as described so far V is equal to the entire volume of an isopycnal slab, from the southern outcrop to the northern continental boundary, and the resulting mass is the total anthropogenic carbon mass in the slab. However, to compute spatial ΔDIC distributions we estimate averaged concentrations $\Delta\mathrm{DIC}_V$ over a series of volumes V defined to the north by successively decreasing CFC12 concentration contours. This formulation allows us to construct the spatial distributions, while at the same time enforcing certain global constraints. If $\Delta M^{\sigma}_{DIC}(V) = V \times \Delta\mathrm{DIC}_V$ is the anthropogenic carbon mass in volume V of an isopycnal slab σ and $\Delta M^{\sigma}_{DIC}(V + \delta V)$ is the mass in volume $V + \delta V$, then the mean concentration along the volume tube δV parallel to the CFC12 contour is

$$\begin{aligned} \Delta\mathrm{DIC}(V) &= \frac{\Delta M^{\sigma}_{DIC}(V+\delta V) - \Delta M^{\sigma}_{DIC}(V)}{\delta V} \\ &\approx \frac{d\Delta M^{\sigma}_{DIC}(V)}{dV}. \end{aligned} \tag{5}$$

We then transform from V coordinates to "CFC12 equivalent latitude," the latitude that encompasses the same volume as the CFC12 contour defining V. Because CFC12 contours are oriented approximately zonally, the CFC12 equivalent latitude is similar to true latitude.

In this manner we can form maps of the inferred ΔDIC that approximate zonally-averaged latitude-depth distributions. We can also plot the inferred ΔDIC on each isopycnal versus longitude and latitude. Because we compute mean concentrations of ΔDIC (minimum to maximum) on CFC contours, the resulting ΔDIC contours on an isopycnal are, by definition, parallel to the CFC12 contours. Components of the ΔDIC distribution perpendicular to CFC12 are unavailable from CFC12 data alone. However, contours of column ΔDIC, formed from vertical integration over the isopycnals, are not necessarily parallel to contours of column CFC12. The CFC12 contour orientations vary with isopycnal, and the fractional contribution of an isopycnal to ΔDIC column values is not generally the same as its fractional contribution to CFC12 column values.

The approach of estimating volume-averaged ΔDIC is a modification of the technique described in *Hall et al.* [2002], who used tracer data to constrain the distributions of transit times, $\mathcal{G}(r,t)$, from the surface to particular locations r. We could follow that approach here to obtain point-wise estimates of ΔDIC, and then integrate spatially to arrive at total mass. However, such a procedure does not take advantage of a global constraint on $\mathcal{G}_V(t)$ (the spatial integral of $\mathcal{G}(r,t)$), namely, that $\mathcal{G}_V(t)$ is a monotonically decreasing function of t when V represents the entire closed domain of the isopycnal slab. In the approach employed here this constraint is enforced because the functional form for $\mathcal{G}_V(t)$ is monotonically decreasing. Thus, in cases such as the Indian Ocean where we have tracer data covering the entire domain we use the approach developed here, while in cases where we analyze spatially limited data removed from the surface source, we use the *Hall et al.* [2002] approach.

3. Results

3.1. Inventory and Uptake

We now apply this technique to compute the total mass, net air-sea flux, and spatial distribution of anthropogenic carbon in the Indian Ocean. To the degree the transport is in steady-state, the constraint on ΔDIC imposed by 1995 CFC12 observations applies over the entire industrial era. We find that the mass of anthropogenic carbon and its net air-sea flux have risen nearly steadily in the industrial era (Fig. 3). In the year 2000 we estimate that the ΔDIC mass was 14.3–20.5 Gt and the net air-sea flux was 0.26–0.36 Gt/yr. The ranges are a result of the imperfect constraint CFC12 imposes on ΔDIC in the presence of mixing, due to the tracers' different histories. They do not represent statistical uncertainty, and no intermediate "best estimate" is available.

Allowing for mixing significantly reduces the estimate of mass and net air-sea flux of anthropogenic carbon. For the Indian Ocean in 2000 the strong-mixing limit is lower than the no-mixing limit by 6.2 Gt in mass and 0.12 Gt/yr in net air-sea flux, reductions of 30% at constant disequilibrium. The effect of mixing can be understood by examining the analyses that have neglected it. Typically, a tracer "age" is defined as the time since the observed concentration of a tracer at an interior location was last exhibited at the surface. For example, $\mathrm{CFC12}(t) = \mathrm{CFC12}_S(t - T_{CFC})$, defining the CFC12 age, T_{CFC}. The tracer age is then applied to the surface history of anthropogenic carbon to estimate the concentration of ΔDIC at the location: $\Delta\mathrm{DIC}(t) = \Delta\mathrm{DIC}_S(t - T_{CFC})$. In the absence of mixing this is valid because there is a unique transit time from the surface source region to the interior location, and the age of any tracer equals this transit time. In the presence of mixing, however, there is a wide distribution of transit times since water at the interior location was last at the surface, and the tracer age is an average over the distribution, weighted by the tracer's history [*Waugh et al.*, 2003a]. The age of a tracer such as CFC12, whose history is shorter and more nonlinear than ΔDIC, preferentially weights young components of the transit-time distribution. The ΔDIC surface history is evaluated at too recent a date, and the interior ΔDIC concentration is overestimated [*Hall et al.*, 2002].

The no-mixing values are upper bounds on the mass and net air-sea flux of anthropogenic carbon (Fig. 3), but using

CFC12 alone they are not ruled out. The simultaneous use of another tracer with a sufficiently distinct history imposes additional, independent constraints on $\mathcal{G}_V(t)$ and narrows the range of ΔDIC mass and net air-sea flux. Unfortunately, given uncertainties in the construction of inventories from sparse data, CFC11 and CFC12 are too similar to provide independent constraints on total ΔDIC mass and net air-sea flux, while the peak in bomb-tritium history is too broad and weak in the southern hemisphere for its attenuation to offer much additional constraint.

However, if one restricts attention to diagnosing transport to locations of observation, rather than over the entire Indian Ocean domain, then formation of inventories is unnecessary, and CFC11 and CFC12 data can be be used constructively in combination [*Waugh et al.*, 2003a]. Fig. 4 shows a scatter plot of the difference of CFC11 and CFC12 concentration ages, $\tau_{11} - \tau_{12}$, versus the CFC12 concentration age, τ_{12}, for all data along the Indian Ocean WOCE line IO3, a longitudinal transect at 20°S. If transport from the surface to the points along the transect were purely bulk advective, then τ_{11} would equal τ_{12} everywhere, and the observations in Fig. 4 would fall along the zero line. This is clearly not the case. Mixing must play a role in the transport.

To quantify the role of mixing we follow of *Waugh et al.* [2003a] and use the two-parameter IG form for $\mathcal{G}(t)$ (as opposed to $\mathcal{G}_V(t)$) to model the IO3 CFC11 and CFC12 data. Surface time histories were constructed from the observed T and S, the solubility functions of *Warner and Weiss* [1985], and the atmospheric histories of *Walker et al.* [2000]. (In this case, rather than scaling the CFC histories by objectively-mapped outcrop concentrations as done for the inventory and uptake calculations, we simply assume the saturations to be 100%.) The surface histories are convolved with the IG $\mathcal{G}(t)$, whose parameters are selected such that the modeled τ_{12} matches the observed τ_{12} and P is constant along the transect. The curves in Fig. 4 correspond to different assumed values of P. In the limit of high P (no mixing), the modeled CFC11-CFC12 relationship collapses to the zero line. By contrast, the curves for $P \leq 10$ match the observed CFC11-CFC12 relationship in detail, with the best fits occurring for $P \leq 1$. (Curves with $P \leq 1$ fall too close together to be distinguished by the data.) Analysis of other WOCE Indian Ocean transects reveal similar behavior.

Although we have not directly used CFC11 and CFC12 in combination to constrain ΔDIC inventory and uptake, the behavior shown in Fig. 4 strongly suggests that Indian Ocean transport is well outside the no-mixing, bulk-advective limit. As shown in Fig 3c, $P \leq 1$ places the domain-mean ΔDIC concentration in the lower half of the range determined from CFC12 alone. This is in agreement with the analysis of *Waugh et al* [2003b] of CFCs and tritium in combination in the subpolar North Atlantic Ocean, who obtained transit-time distributions in the strong-mixing limit and, consequently, ΔDIC concentrations significantly lower than estimates from studies making the no-mixing assumption.

Permitting variable disequilibrium further reduces the estimates of ΔDIC mass and net air-sea flux. ΔDIC is allowed to leave the mixed layer before equilibrating with new, higher atmospheric CO_2 levels, and, thus, its surface history is reduced. The largest effect is found on the intermediate isopycnal, $\sigma_0 = 26.7$, where ΔDIC at the surface outcrop is reduced in 2000 by 10%–12% (Fig. 5). (When the disequilibrium is allowed to vary, $\Delta\text{DIC}_S(t)$ itself becomes a function of transport. Pure bulk advection is more effective than mixing at pulling material away from the surface, and so $\Delta\text{DIC}_S(t)$ at high P is more reduced from constant disequilibrium, in this case 12% compared to 10%.) The reduced surface history is transported to the interior, resulting is lower ΔDIC mass. Providing for time-dependent disequilibrium reduces the estimate of Indian Ocean ΔDIC mass in 2000 by 0.9 Gt for strong mixing and by 1.8 Gt for no mixing, fractional reductions of 5%–10% compared to the no-mixing, constant-disequilibrium result (Fig. 3). The fractional reductions in net air-sea flux are similar.

3.2. Uncertainties

There are several sources of uncertainty in our analysis. A first source comes from the objective mapping of CFC12 from sparse cruise lines to gridded values on isopycnals. (CFC12 measurement uncertainty itself is negligible.) This mapping introduces uncertainty in the CFC12 isopycnal-mean concentrations, which propagates nearly directly to uncertainty in inferred ΔDIC. This can be seen simply by mapping a uncertainty range of CFC12_V on the x-axis of Fig 2c to a range of ΔDIC_V on the y-axis. The objective mapping routine applied to the CFC12 data provides an uncertainty for the CFC12 inventory on each isopycnal surface. These uncertainties varied from 7% to 16%, with a value of 14% for $\sigma_0 = 26.7$, the surface having the largest CFC12 and ΔDIC inventories.

A second source of error comes from our neglect of Red Sea (RS) sources of tracer into the Indian Ocean thermocline. In order to put an upper bound on the ΔDIC from these sources we first note that *You and Tomczak* [1993] estimate about 2% of the Indian Ocean thermocline to have RS origin. The fractional contribution to the ΔDIC inventory may be higher, because the ΔDIC contribution increases with T and S. To estimate the maximum possible RS ΔDIC contribution, we make the unrealistic assumption that RS water spreads instantaneously throughout the thermocline, so that all RS water carries the most recent (and highest) possible ΔDIC mole fraction. For $T = 27^\circ$ and $S = 40$ typical of the RS, this is ΔDIC(2000)= 66μmole/kg. Thus, the upper bound on the RS contribution to the inventory is $0.02\times66\times V = 0.9$ Gt, where $V = 5.3\times10^7$ km^3 is the Indian Ocean thermocline volume computed from the objectively-mapped isopycnic depth fields. This mass represents 4% to 6% of our range on Indian Ocean ΔDIC inventory.

In reality the RS contribution will be significantly smaller than the 0.9 Gt upper bound. Firstly, the RS source takes a finite time to propagate through the thermocline, so that much of its water mass is aged and carries an older, lower ΔDIC signal. Secondly, there is a partially compensating error due to the neglect of RS sources of CFC12. We have assumed that the entire CFC12 inventory originates in the south, and have therefore overestimated the role of the southern CFC12 source. This causes our estimate of the TTD from southern sources to be biased young, which in turn causes an overestimate of the southern ΔDIC source. This overestimate is of the same order as the underestimate due to direct neglect of the RS ΔDIC source, so that there is a tendency for these errors to cancel.

While the RS source is only a small contributor to the total Indian Ocean inventory, it is a significant contributor locally in the Arabian Sea. Therefore, our neglect of an RS

source causes our inferred ΔDIC distributions in the Arabian Sea to be biased low, possibly by one third (a 5% total inventory error confined to 15% of the total volume).

A third source of uncertainty arises from the imperfectly known CFC12 histories at the southern outcrops. We have used the objectively-mapped 1995 observations at the outcrops to scale the atmospheric CFC12 history of *Walker et al.* [2000], which provides a boundary condition that implicitly includes CFC12 disequilibrium. However, the objective mapping is least accurate in the Southern Ocean, where the observations are most scarce. Moreover, the measurement are not generally made during the season of subduction. To make a rough estimate of the impact on ΔDIC of these uncertainties we repeated the calculations using an equilibrium solubility calculation (100% saturation) for the CFC12 outcrop histories, given the observed T and S. This results in a change to the 1995 ΔDIC inventory of about 1.7 Gt, or 13% to 9% (strong- to no-mixing limits).

A fourth source of uncertainty arises from the selection of a particular functional form for the TTD. This uncertainty is very difficult to quantify. However, because the IG form used here can closely mimic TTDs simulated directly in numerical models (Appendix A) we think that its selection incurs an error small compared to other sources of uncertainty. In any case, the IG form is a step beyond the assumption of no-mixing that is implicit in previous studies that use tracer ages to lag ΔDIC time series.

Finally, all techniques to estimate anthropogenic carbon concentrations in the ocean assume that ΔDIC propagates as a passive, inert tracer in a steady-state circulation. This assumption causes error in ΔDIC inference to the extent that ocean biota are evolving in response to increased carbon levels and ocean circulation is evolving in response to global warming. At present, these effects are likely small compared to other uncertainties, but their importance will grow in future [e.g., *Saramiento et al.*, 1998].

3.3. Comparison to Other Estimates

The upper bounds of our estimate ranges of anthropogenic carbon mass in the Indian Ocean and its net air-sea flux just encompass those of other studies, while the lower bounds are significantly lower than other studies (Fig. 3), due to the relaxation of the widely-made assumptions of no mixing and constant disequilibrium which cause positive bias. *Sabine et al.* [1999] estimated a 1995 mass of 20.3±3 Gt C, compared to our 13.1–18.8 Gt C. The central value of their range falls very close to our 1995 no-mixing, constant-disequilibrium curve, consistent with expectation, as the *Gruber et al.* [1996] technique used by *Sabine et al.* [1999] makes these approximations. (*Gruber et al.* [1996] make the no-mixing assumption by using tracer ages to estimate disequilibrium terms, which are assumed to be constant. They reduce sensitivity to the no-mixing assumption by restricting application to waters with tracer ages less than a threshold.) *McNeil et al.* [2003], who also make these approximations by applying CFC12 ages directly to ΔDIC surface history assuming constant disequilibrium, estimated a net air-sea flux into the Indian Ocean averaged over the interval 1980-1989 of 0.31 Gt C/yr and over the interval 1990-1999 of 0.37 Gt C/yr, compared to our ranges of 0.22–0.28 Gt C/yr and 0.24–0.34 Gt C/yr, respectively. Their estimates also fall on our constant-disequilibrium, no-mixing curve.

Our bounds on the spatial distribution of ΔDIC concentration are shown in Fig 6. ΔDIC penetrates most deeply in southern midlatitudes, the zone of subtropical convergence, while below 800 m in the northern Indian Ocean there is little ΔDIC. This latitude-depth distribution is qualitatively similar to those of *Sabine and Feely* [2001], who compared the techniques of *Gruber et al.* [1996] and *Chen and Millero* [1979], although there are numerous differences in detail. Our latitude-longitude distribution of column inventories has an upper bound (no mixing) that peaks in southern midlatitudes at about 40 mol/m^2 and decreases to about 15 mol/m^2 in the Bay of Bengal. This is similar in shape, but slightly lower in magnitude than the column distribution estimated by *Sabine and Feely* [2001] using the *Gruber et al.* [1996] method. Our lower bound (strong mixing) is lower still, ranging from about 30 mol/m^2 to below 10 mol/m^2. The *Sabine and Feely* [2001] distribution using the *Chen and Millero* [1979] method has a significantly stronger latitudinal gradient, ranging from above 55 mol/m^2 to below 10 mol/m^2.

A comparison of the mean vertical ΔDIC concentration profile estimated by *Sabine et al.* [1999] to our inferred range is shown in Fig. 7. *Sabine et al.* [1999] used the inference method of *Gruber et al.* [1996]. In this method, on isopycnals that are believed to be everywhere contaminated by anthropogenic carbon, tracer ages (e.g., CFC ages) are used to estimate the ΔDIC air-sea disequilibrium, which amounts to a neglect of mixing. The disequilibrium is overestimated, leading to an underestimate of the preindustrial background, and, consequently, an overestimate of the anthropogenic component of total observed DIC overestimated (see *Hall et al.* [2002] for a more detailed discussion of this bias). In addition, the disequilibrium is assumed to be constant in time. Thus, we expect the *Sabine et al.* [1999] ΔDIC profile to exhibit a high bias in shallow regions. On the other hand, for deeper isopycnals that are believed to have regions old enough to be uncontaminated by ΔDIC *Gruber et al.* [1996] use measured DIC in these old regions as the preindustrial background to be subtracted from total DIC. If mixing brings small amounts of ΔDIC into these old regions, then the preindustrial DIC is overestimated, and ΔDIC underestimated. Thus, we expect the *Sabine et al.* [1999] profile to be biased low in deeper waters.

The *Sabine et al.* [1999] profile is, in fact, greater than our range above 950 m (except near the surface) and less than our range below 1200 m. While this behavior is generally consistent with expectation, the magnitude of the differences between 950 and 150 m cannot be explained solely by the no-mixing and constant-disequilibrium biases. The no-mixing bias alone would put the *Sabine et al.* [1999] profile at most on our upper bound, and the constant-disequilibrium bias is only a 5%–10% effect (section 3.1). By contrast, at 600 m, the *Sabine et al.* [1999] ΔDIC concentration is about 50% greater than our upper bound. We note that the *Gruber et al.* [1996] method makes use of Redfield ratios, R, in the construction of a quasi-conservative DIC tracer. *Wanninkhof et al.* [1999] have shown that realistic uncertainties in R can lead to large fractional errors at moderate ΔDIC concentrations, which might explain some of the discrepancy. On the other hand, we have neglected ΔDIC sources from the Red Sea. While this causes an underestimate in the total Indian Ocean inventory of less than 6% (section 3.2), the fractional error for the mean concentration north of 35° is somewhat higher.

4. Summary

We have developed and applied to the Indian Ocean a new technique to infer the distribution, inventory, and net air-sea flux of anthropogenic carbon. Observations of CFC12 are used to constrain distributions of transit times from the surface to the interior that are designed to accommodate any proportion of diffusive mixing and bulk advection. The transit-time distributions are then used to propagate into the interior the surface-water history of anthropogenic carbon estimated in a way that includes the natural temporal variation in CO_2 air-sea disequilibrium. By allowing for mixing in transport and temporal variation in the air-sea CO_2 disequilibrium, our technique removes two sources of positive bias found in most other studies.

We estimate that the anthropogenic carbon mass in the Indian Ocean was 14.3–20.5 Gt in 2000, and the net air-sea flux was 0.26–0.36 Gt/yr, with the low and high ends of the ranges representing strong- and no-mixing transport limits. The ranges reflect the imperfect constrain that CFC12 imposes on anthropogenic, due to the tracers' different histories. Our no-mixing estimates for the total mass and net air-sea flux of anthropogenic carbon in the Indian Ocean are in approximate agreement with other studies [*Sabine et al.* 1999; *McNeil et al.*, 2003], while our strong-mixing estimates are significantly lower. Preliminary analysis of CFC11 and CFC12 in combination suggests that Indian Ocean transport is well outside the no-mixing limit, and, consequently, that ΔDIC inventory and uptake is in the lower half of its range, in agreement with a similar analysis in the subpolar North Atlantic [*Waugh et al.*, 2003b].

We have analyzed the Indian Ocean, whose contribution to the global ocean uptake of anthropogenic carbon is the order of 20% [*Takahashi et al.,* 2002; *McNeil et al.,* 2003]. The biases shown here to be incurred in the Indian Ocean by the widely-made assumptions of no mixing and constant disequilibrium are also relevant to other oceans. If the relaxation of these assumptions in other oceans leads to similar downward expansion in the estimated range ΔDIC then the lower bounds on estimated ΔDIC mass in the global ocean would have to be reduced by about a third. Even the upper bound of our uptake range, which agrees roughly with *McNeil et al.* [2003], is below the uptake predicted by many general circulation models [*McNeil et al.*, 2003; *Orr et al.*, 2001]. Uptake values at the lower end of our range would further exacerbate the discrepancy with these models.

Appendix

Here, we motivate and describe the two-parameter functional form used for the TTD. Every parcel of water has a transit-time distribution (TTD) since it was last at the surface. In the case of pure bulk-advection the TTD is a narrow spike at a single transit-time, the advective timescale. More generally, the TTD is broadly distributed, due to mixing.

A useful functional form for the TTD is the two-parameter "inverse Gaussian" (IG) form used, for example, by *Hall et al* [2002] and *Waugh et al.* [2003a]. The IG form is the boundary-propagator solution to a semi-infinite one-dimensional advection-diffusion equation with constant coefficients. That is, it is the solution with no interior sources and a boundary condition of $\mathcal{G}(t) = \delta(t)$, where $\delta(t)$ is the Dirac delta function. The IG form, however, has utility beyond idealized one-dimensional models, and is a common statistical tool in the analysis of right-skewed data [*Seshadri*, 1999]. TTDs simulated directly in ocean general circulation models generally have early peaks, representing advective transport along some dominant pathway, and long tails, due to along-flow and lateral mixing [e.g., *Khatiwala et al.*, 2001; *Haine and Hall*, 2002; *Primeau*, 2003]. While the circulation is complex and two- or three-dimensional, the TTD can often (but not always) be well fit by the IG form.

In this study we want to parameterize the TTD averaged over a volume that includes, as one boundary, the surface source region. That is, we want to parameterize

$$\mathcal{G}_V(t) \equiv \frac{1}{V}\int_V d^3r\, \mathcal{G}(r,t) \qquad \text{(A-1)}$$

$\mathcal{G}_V(t)$ is the distribution of transit times since water in the volume V (one boundary of which is the surface source region) made last contact with the surface source region. The IG form for $\mathcal{G}_V(t)$ is obtained by averaging the IG form over a one-dimensional "volume" extending from the origin to some position whose value is expressed in terms of mean transit-time. One obtains functional form (1) whose parameters are τ, twice the mean transit time ("mean age") of all the fluid elements in V, and P, the Peclet number, defined as the ratio of diffusive to advective timescales.

While the volume-TTD of real ocean domains may differ considerably in detail from the IG form, there are certain general properties of volume-TTD that the IG form captures: 1. For a closed domain $\mathcal{G}_V(t)$ is a non-increasing function of t [*Haine and Hall*, 2002], simply the statement that every parcel at transit time ("age") t must have passed through every earlier transit time. 2. $\mathcal{G}_V(t)$ is singular at $t = 0$ [*Holzer and Hall*, 2000]. 3. The large t limit of $\mathcal{G}_V(t)$ is exponential decay [*Haine and Hall*, 2002].

To illustrate of utility of the volume-IG form we have fit it to the $\mathcal{G}_V$ simulated directly in a two-dimensional Stommel gyre model and a general circulation model (GCM). The Stommel gyre model is configured as in *Thiele and Sarmiento* [1991]. Figure A1a and A1b show $\mathcal{G}_V(t)$ for the whole 2-D model domain in two sample circulations, fast and slow. Also shown are best-fit IG forms, which have the paremeters $\tau = 15$ years and $P = 16$ for the fast circulation and $\tau = 48$ years and $P = 7.6$ for the slow circulation. Figure A1(c) shows the $\mathcal{G}_V(t)$ for sub-tropical mode water in the North Atlantic, as simulated by *Haine and Hall* [2002] using an ispocnal GCM. (The $\mathcal{G}_V(t)$ of Figure A2c is equivalent to that shown in Figure 8d of Haine and Hall, but plotted on a linear scale.) The best fit IG has the parameters $\tau = 22$ years and $P = 1.7$. In all three cases the IG form closely mimics the directly-simulated TTD, giving us confidence in its application to observational data.

Acknowledgments. We thank M. Follows for his equilibrium inorganic carbon system code, Bill Smethie for discussions on CFC inventory uncertainties, and Chris Sabine and an anonymous reviewer for comments that led to an improved manuscript. This work was supported in part by a grant from the National Science Foundation OCE physical oceanography program.

5. References

Beining, P., and W. Roether, Temporal evolution of CFC 11 and CFC 12 concentrations in the ocean interior, *J. Geophys. Res., 101,* 16,455–16,464, 1996.

Bower, A. S., H. D. Hunt, and J. F. Price, Character and dynamics of the Red Sea and Persain Gulf outflows, *J. Geophys. Res., 105,* 6387–6414, 2000.

Brewer, P. G., Direct measurement of the oceanic CO_2 increase, *Geophhys. Res. Lett., 5,* 997-1000, 1978.

Carr, M.-E., W. Tang, and W. T. Liu, CO_2 exchange coefficients from remotely sensed wind speed measurements: SSM/I versus QuikSCAT in 2000, *Geophys. Res. Lett., 29,* doi:10.1029/2002GL015068, 2002.

Chen, C.-T., and F. J. Millero, Gradual increase of oceanic CO_2, *Nature, 277,* 205–206, 1979.

Coatanoan, C., C. Goyet, N. Gruber, C. L. Sabine, and M. Warner, Comparison of two approaches to quantify anthropogenic CO_2 in the ocean: Results from the northern Indian Ocean, *Global Biogeochem. Cycles, 15,* 11–25, 2001.

Etheridge, D. M., et al., Historical CO_2 records from the Law Dome DE08, DE08-2, and DSS ice cores. In *Trends: A Compendium of Data on Global Change,* Carbon Dioxide Information Analysis Center, Oak Ridge National Laboratory, Oak Ridge, Tenn., 1998.

Fine, R., J. L. Reid, and H. G. Ostlund, Circulation of tritium in the Pacific Ocean, *J. Phys. Oceanogr., 11,* 3–14, 1981.

Goyet, C., C. Coatanoan, G. Eischeid, T. Amaoka, K. Okuda, R. Healy, and S. Tsunogi, Spatial distribution of total CO_2 and total alkalinity in the northern Indian Ocean: A novel approach for the quantification of anthropogenic CO_2 in seawater, *J. Mar. Res., 57,* 135–163, 1999.

Goyet, C., and P. G. Poisson, New determination of carbonic acid dissociation constants in seawater as a function of temperature and salinity, *Deep-Sea Res., 36,* 2635–2654, 1989.

Gruber, N., J. L. Sarmiento, and T. F. Stocker, An improved method for detecting anthropogenic CO_2 in the oceans, *Global Biogeochem. Cycles, 10,* 809–837, 1996.

Haine, T. W. N., and T. M. Hall, A generalized transport theory: Water-mass composition and age, *J. Phys. Oceanogr., 32,* 1932–1946, 2002.

Hall, T. M., T. W. N. Haine, and D. W. Waugh, Inferring the concentration of anthropogenic carbon in the ocean from tracers, *Global Biogeochem. Cycles, 16*, doi:10.1029/2001GB001835, 2002.

Holzer, M., and T. M. Hall, Transit-time and tracer-age distributions in geophysical flows, *J. Atmos. Sci., 57,* 3539–3558, 2000.

Jenkins, W. J., The use of anthropogenic tritium and helium-3 to study subtropical gyre ventilation and circulation, *Phil. Trans. R. Soc. Lond. A*, 325, 43–61, 1988.

Karstensen, J., and D. Quadfasel, Water subducted into the Indian Ocean subtropical gyre, *Deep-Sea Res. II, 49,* 1441–1457, 2002.

Khatiwala, S., M. Visbeck, and P. Schlosser, Age tracers in an ocean GCM, *Deep-Sea Res. I, 48,* 1423–1441, 2001.

Lewis, E., and D. W. R. Wallace, Program developed for CO_2 system calculations, *ORNL/CDIAC-105*, Carbon Dioxide Inf. Anal. Cent., Oak Ridge Natl. Lab., U. S. Dep. of Energy, Oak Ridge, Tenn, 1988.

Matear, R. J., C. S. Wong, and L. Xie, Can CFCs be used to determine anthropogenic CO_2, *Global Biogeochem. Cycles, 17,* doi:10.1029/2001GB001415, 2003.

McNeil, B. I., R. J. Matear, R. M. Key, J. L. Bullister, and J. L. Sarmiento, Anthropogenic CO_2 uptake by the ocean based on the global chlorofluorocarbon data set, *Science, 299,* 235–239, 2003.

Orr, J. C., et al., Estimates of anthropogenic carbon uptake from four three-dimensional global ocean models, *Global Biogeochem. Cycles, 15,* 43–60, 2001.

Primeau, F., Characterizing transport between the surface mixed layer and the ocean interior with a forward and adjoint global ocean transport model. *J. Phys. Oceanogr.,* (submitted), 2003.

Robbins, P. E., J. F. Price, W. B. Owens, and W. J. Jenkins, On the importance of lateral diffusion for the ventilation of the lower thermocline in the subtropical North Atlantic, *J. Phys. Oceanogr., 30,* 67–89, 2000.

Sabine, C. L., et al., Anthropogenic CO_2 inventories in the Indian Ocean, *Global Biogeochem. Cycles, 13,* 179–198, 1999.

Sabine, C. L., and R. A. Feely, Comparison of recent Indian Ocean anthropogenic CO_2 estimates with a historical approach, *Global Biogeochem. Res., 15,* 31–42, 2001.

Sarmiento, J. L, T. M. C. Hughes, R. J. Stouffer, and S. Manabe, Simulated response of the ocean carbon cycle to anthropogenic climate warming, *Nature, 393,* 245–249, 1998.

Seshadri, The inverse Gaussian distribution: Statistical theory and applications, Springer-Verlag, New York, 1999.

Sonnerup, R. E., On the relations among CFC derived water mass ages, *Geophys. Res. Lett., 28,* 1739–1742, 2001.

Takahashi, T., et al., Global air-sea CO_2 flux based on climatological surface ocean pCO_2 and seasonal biological and temperature effects, *Deep-Sea Res. II, 49,* 1601–1622, 2002.

Thiele, G., and J. L. Sarmiento, Tracer dating and ocean ventilation, *J. Geophys. Res., 95,* 9377–9391, 1990.

Thomas, H., and V. Ittekkot, Determinationn of anthropogenic CO_2 in the North Atlantic Ocean using water mass age and CO_2 equilibrium chemistry, *J. Mar. Systems, 27,* 325–336, 2001.

Thomas, H., M. H. England, and V. Ittekkot, An off-line 3D model of anthropogenic CO_2 uptake by the oceans, *Geophys. Res. Lett., 28,* 547–550, 2001.

Walker, S. J. et al., Reconstructed histories of the annual mean atmospheric mole fraction for the halocarbons CFC11, CFC12, CFC113 and carbon tetrachloride, *J. Geophys. Res., 105,* 14,285–14,296, 2000.

Wanninkhof, R., Relationship between wind speed and gas exchange ovver the oceann, *J. Geophys. Res., 97,* 7373–7382, 1992.

Wanninkhof, R., S. C. Doney, T.-H. Peng, J. L. Bullister, K. Lee, and R. A. Feely, Comparison of methods to determine the anthropogenic CO_2 invasion into the Atlanntic Ocean, *Tellus Ser. B, 51,* 511–530, 1999.

Warner, M. J., and R. F. Weiss, Solubilities of chlorofluorocarbons 11 and 12 in water and sea water, *Deep-Sea Res., A, 32,* 1485–1497, 1085.

Waugh, D. W., T. M. Hall, and T. W. N. Haine, Relationships among tracer ages, *J. Geophys. Res., 108,* doi:10.1029/2002JC001325., 2003a.

Waugh, D. W., T. W. N. Haine, and T. M. Hall, Transport times and anthropogenic carbon in the subpolar North Atlantic Ocean, *Deep-Sea Res.*, 2003b (submitted).

You, Y., and M. Tomczak, Thermocline circulation and ventilation in the Indian Ocean derived from water mass analysis, *Deep Sea Res. I, 40,* 13-56, 1993.

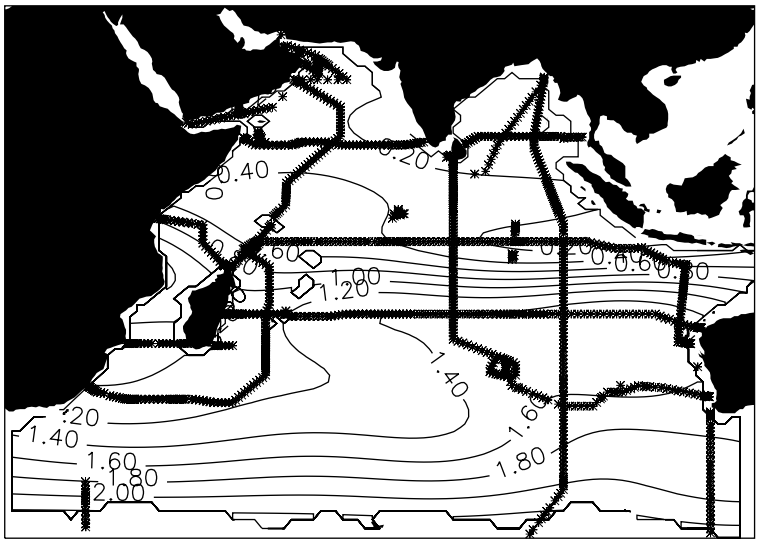

Figure 1.

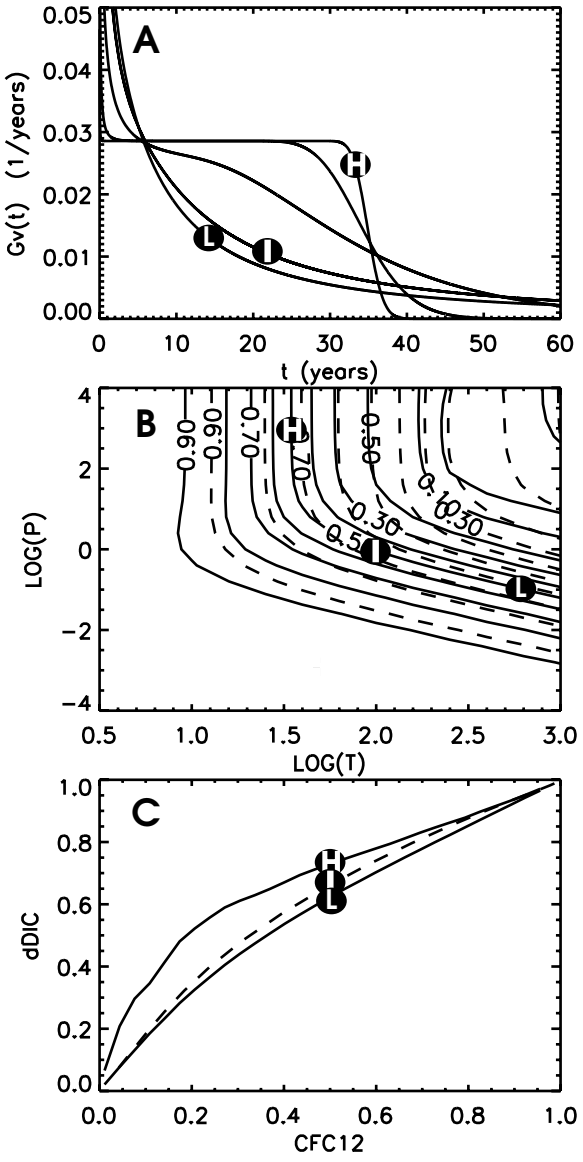

Figure 2.

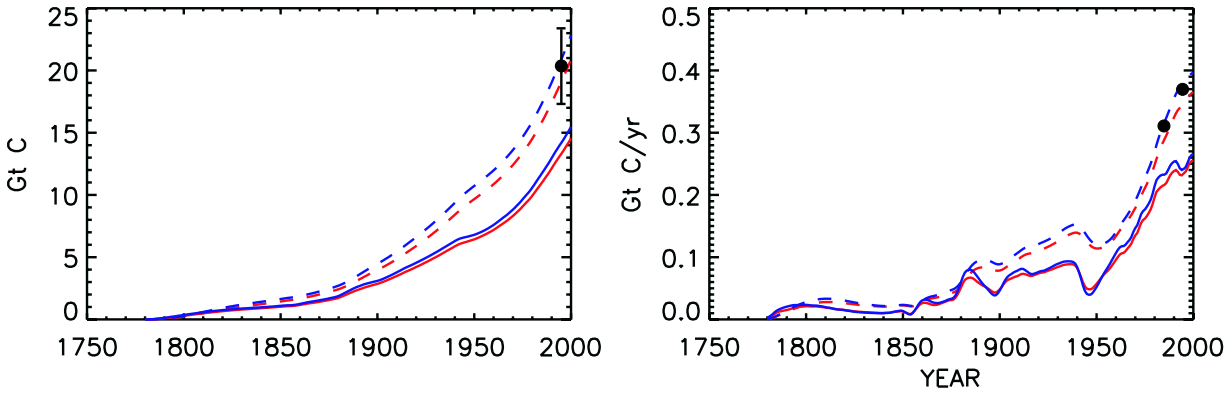

Figure 3.

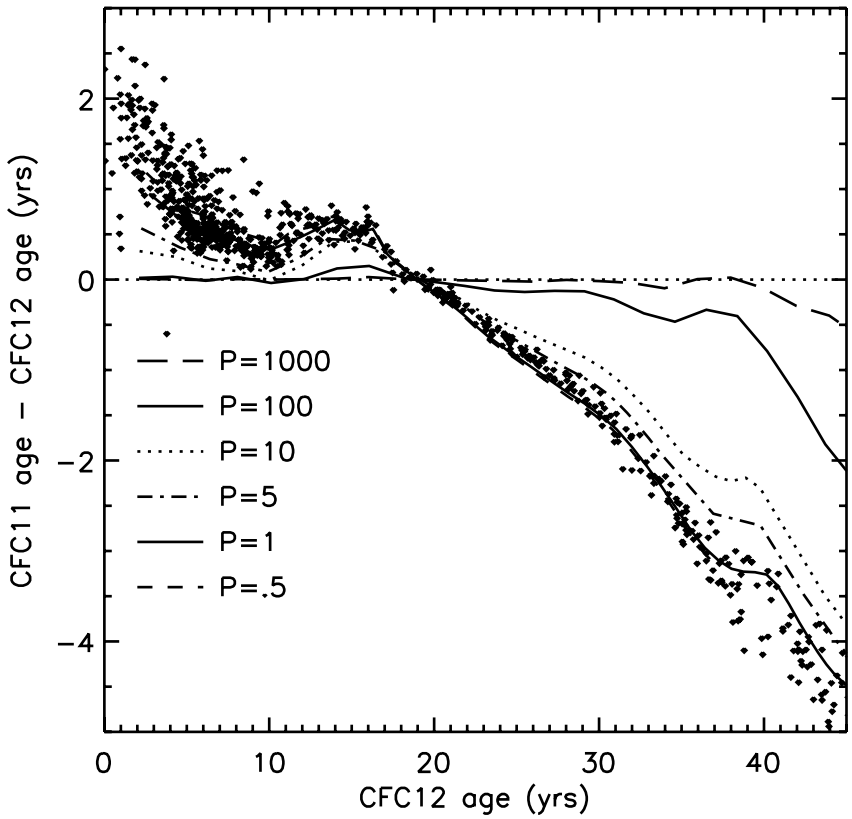

Figure 4.

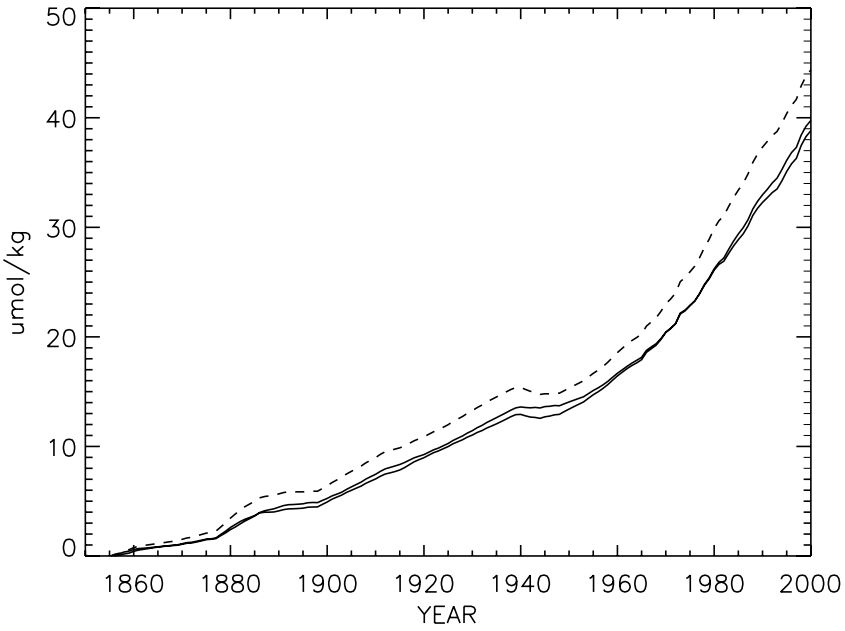

Figure 5.

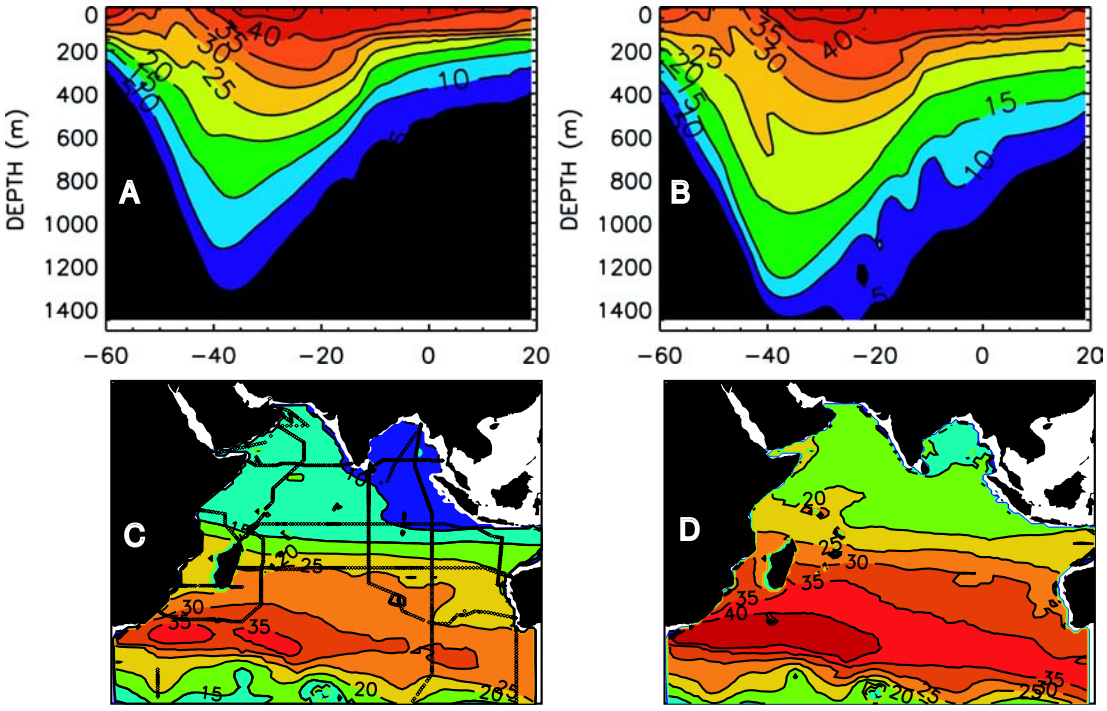

Figure 6.

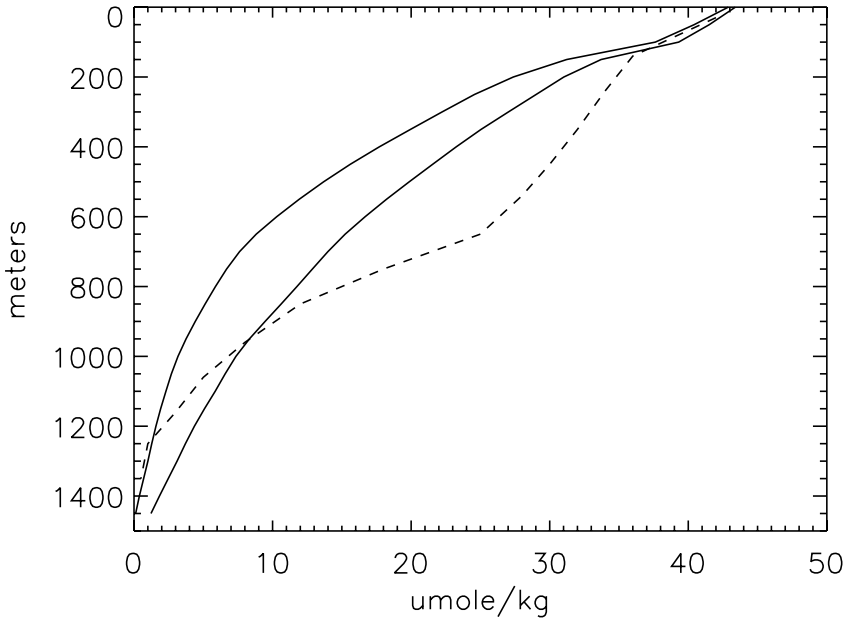

Figure 7.

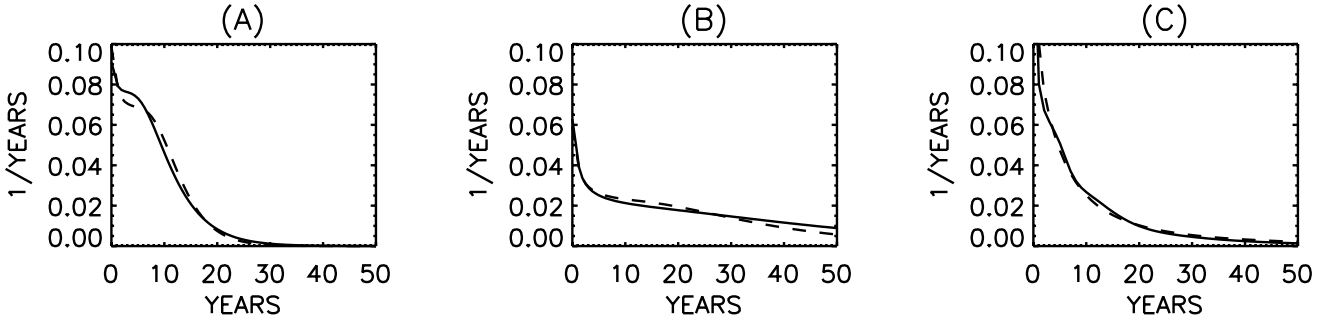

Figure 1.

Figure 1: CFC12 concentration (pmole/l) on the $\sigma_0 = 26.7$ isopycnal. The crosses indicate the locations of WOCE CFC12 measurements from which the distributions are formed.

Figure 2: (a) Examples of $\mathcal{G}_V(t)$ that give rise to identical $\mathrm{CFC12}_V$. "H" is in the high P limit ($P = 1000$ and $\tau = 35$ years); "I" is intermediate ($P = 1$ and $\tau = 96$ years); and "L" is in the low P limit ($P = 0.1$ and $\tau = 630$ years). Two other $\mathcal{G}_V(t)$ are shown between "H" and "I" ($P = 100$, $\tau = 35$ years and $P = 10$, $\tau = 40$ years). (b) $\mathrm{CFC12}_V$ (solid) and $\Delta\mathrm{DIC}_V$ (dashed) versus τ and P on log scales, expressed as fractions of their contemporary concentrations at the outcrop. The locations of the three $\mathcal{G}_V(t)$ labeled in panel A are shown. (c) Relationship between $\mathrm{CFC12}_V$ and $\Delta\mathrm{DIC}_V$ from the contour intersections in panel B, expressed as fractions of contemporary concentrations at the outcrop (solid). The $\mathrm{CFC12}_V\Delta\mathrm{DIC}_V$ relationship for $P = 1$ (dashed curve) and the values corresponding to the three labeled $\mathcal{G}_V(t)$ are shown.

Figure 3: (a) Total ΔDIC mass in the Indian Ocean and (b) net air-sea flux into the Indian Ocean. In both panels, blue curves are derived from constant disequilibrium, while red curves are for time-varying disequilibrium. The dashed curves are the high P (no mixing) limit and the solid curves the low P (strong mixing) limit. In (a), the symbol with uncertainty bar (20.3±3 Gt) is the estimate of *Sabine et al.* [1999]. In (b) the symbols are the estimates from *McNeil et al.* [2003] of net flux averaged over 1980-1989 (0.31 Gt C/yr) and 1990-1999 (0.37 Gt C/yr).

Figure 4: The difference of CFC11 and CFC12 concentration age plotted as a function of CFC12 concentration age. The symbols are from observations along WOCE transect IO3 (longitudinal transect at 20°S). The curves are fits to the data using the IG form for $\mathcal{G}(t)$ assuming different Peclet numbers, P, as listed in the key.

Figure 5: Time series of ΔDIC surface concentration on the $\sigma_0 = 26.6$ isopycnal assuming constant-disequilibrium (dashed), and allowing time-varying disequilibrium in the no-mixing (lower solid) and strong-mixing (higher solid) limits.

Figure 6: Ranges of the spatial distribution of ΔDIC. (a) Minimum and (b) maximum ΔDIC (μmol/kg) versus equivalent latitude and depth. (c) Minimum and (d) maximum column ΔDIC (mol/m^2) versus longitude and latitude.

Figure 7: Vertical profile of mean ΔDIC concentration north of 35°S, minimum and maximum, as estimated in this study (solid). Comparable profile estimated by *Sabine et al.* [1999] (dashed).
Figure A1: Volume TTDs as computed in three models: (A) Stommel gyre with a fast circulation; (B) Stommel gyre with a slow circulation; and (C) Subtropical mode water in a North Atlantic isopycnal general circulation model. In each case, the dashed lines are the best fits using the IG volume-TTD form. In (A), $\tau = 15$ years and $P = 16$; in (B), $\tau = 48$ and $P = 7.6$; and in (C), $\tau = 22$ years and $P = 1.7$.